Industrial Chemistry & Materials

ROYAL SOCIETY OF CHEMISTRY

PAPER

View Article Online
View Journal

Cite this: DOI: 10.1039/d6im00032k

$K(Gd_{0.1}Yb_{0.9})_3F_{10}$, a promising refrigerant for sub-100 mK adiabatic demagnetization refrigeration

Qiao-Fei Xu,†[ab] Peng Zhao,†[c] Man-Ting Chen,[a] Ruo-Tong Wu,[a] Wei Dai,*[c] La-Sheng Long *[a] and Lan-Sun Zheng[a]

Ultralow-temperature refrigeration is indispensable for advancing quantum technologies and astrophysical instrumentation operating below 1 K. Adiabatic demagnetization refrigeration (ADR) offers a reliable and efficient alternative to ^{3}He-based systems, but progress has been limited by the modest magnetic entropy change ($-\Delta S_m$) of commercial refrigerants at sub-kelvin temperatures. Here, we report $K(Gd_{0.1}Yb_{0.9})_3F_{10}$ (**1**), a dense lanthanide fluoride synthesized by partially substituting Gd^{3+} into KYb_3F_{10}, as a high-performance refrigerant for ADR. Owing to weak magnetic interactions and the absence of long-range ordering down to 50 mK, **1** delivers substantial $-\Delta S_m$ values across 0.3–1.0 K. When integrated into a two-stage ADR system, **1** achieves a minimum temperature of 67 mK, a remarkable cooling capacity of 607.82 mJ and load-free operation for over 30 h at 300 mK under a residual magnetic field of 1.03 T. These results position the refrigerator loaded with $K(Gd_{0.1}Yb_{0.9})_3F_{10}$ as a promising alternative to ^{3}He-based systems near 300 mK and underscore its potential for practical helium-free cryogenic applications in quantum technologies and space platforms.

Keywords: Adiabatic demagnetization refrigeration; Ultralow temperatures; Cooling capacity; Two-stage refrigerator.

Received 22nd January 2026,
Accepted 16th April 2026

DOI: 10.1039/d6im00032k

rsc.li/icm

1 Introduction

Adiabatic demagnetization refrigeration (ADR), independent of both ^{3}He resources and gravity,[1–4] provides an effective route to ultra-low temperatures for suppressing thermal fluctuations. It has been widely used to support high-precision transition-edge sensors (TES) in astronomical observations and is being explored for emerging quantum technologies.[5,6] The limited global supply and high cost of ^{3}He[7] have further spurred interest in ADR-based, ^{3}He-free refrigeration as a sustainable route toward scalable ultralow-temperature technologies. ADR relies on the magnetocaloric effect (MCE) of refrigerants, yet its performance is constrained by the limited magnetic entropy change ($-\Delta S_m$) and the efflorescent nature of currently available commercial materials—primarily paramagnetic salts.[8,9] Despite their successful implementation in space missions, classical paramagnetic salts such as CPA and FAA possess relatively low magnetic density and modest entropy per unit volume, which limit the cooling capacity achievable within compact ADR architectures. As detector arrays continue to expand in size and complexity, the associated thermal loads increase accordingly, placing more stringent requirements on cooling power per unit mass and per cycle.[10] Meanwhile, the use of hydrated salts limits the temperature of the baking process typically required by space mission or high vacuum systems.[11] These constraints motivate the exploration of denser stable magnetic refrigerants capable of delivering larger entropy change without sacrificing low ordering temperatures.

To address this limitation, extensive efforts have focused on discovering new refrigerants to improve ADR performance.[12–17] A key milestone was NASA's demonstration of enhanced cooling capacity in the 0.5–4 K range by replacing $Gd_3Ga_5O_{12}$ (GGG) or $CrK(SO_4)_2{\cdot}12H_2O$ (CPA) with $LiGdF_4$.[18,19] Yet, below 0.5 K, $CrK(SO_4)_2{\cdot}12H_2O$ (CPA) and $(NH_4)Fe(SO_4)_2{\cdot}12H_2O$ (FAA) remain the prevalent refrigerants in practical use,[20] despite the discovery of several stable alternatives—such as $NaYbP_2O_7$,[21] $KBaYb(BO_3)_3$[22] and $Na_2BaCo(PO_4)_2$[23]—which can access ultralow temperatures but provide no significant enhancement in $-\Delta S_m$. In addition

[a] Collaborative Innovation Center of Chemistry for Energy Materials, State Key Laboratory of Physical Chemistry of Solid Surfaces, College of Chemistry and Chemical Engineering, Xiamen University, Xiamen 361005, Fujian, China. E-mail: lslong@xmu.edu.cn
[b] Key Laboratory of Functional Molecular Solids Ministry of Education, College of Chemistry and Materials Science, Anhui Normal University, Wuhu, Anhui, 241002, China
[c] State Key Laboratory of Cryogenic Science and Technology, Chinese Academy of Sciences, Technical Institute of Physics and Chemistry, Beijing 100190, China. E-mail: cryodw@mail.ipc.ac.cn
† These authors contributed equally to this work.

to intrinsic magnetic parameters such as entropy change and ordering temperature, practical ADR refrigerants must also exhibit adequate structural stability, chemical robustness, reasonable cost, and sufficient thermal conductivity to enable efficient heat exchange and long-term operation. These considerations further favour dense inorganic frameworks over efflorescent paramagnetic salts. For application in a practical refrigerator, only a few assessments have been published: ESA's $Yb_3Ga_5O_{12}$ and our previously studied $LiGd_{0.1}Yb_{0.9}F_4$.[24,25] In this work, we extend our previously validated Gd-doping strategy in dense frameworks to enhance $-\Delta S_m$ at ultralow temperatures[26] and report here the minimum achievable temperature and cooling capacity of $K(Gd_{0.1}Yb_{0.9})_3F_{10}$ (**1**) under load. Significantly, when integrated into a two-stage ADR system, **1** reached a minimum temperature of 67 mK and delivered a high specific cooling capacity of 47.99 mJ cm^{-3} T^{-1} under 0.27 T, establishing it as a competitive sub-kelvin refrigerant that rivals ^{3}He-based systems. Although the minimum temperatures achieved in the present work remain above the typical operating temperatures required for many quantum computing platforms, the development of ^{3}He-free refrigeration is nonetheless relevant to addressing long-term scalability challenges associated with ^{3}He scarcity.

2 Results and discussion

2.1 Antiferromagnetic $K(Gd_{0.1}Yb_{0.9})_3F_{10}$

The single-crystal X-ray diffraction analysis reveals that **1** crystallizes in the cubic space group $Fm\bar{3}m$ (Fig. 1a and b), similar to that of KYb_3F_{10} with a larger cell volume (Table S1).[27,28] The powder X-ray diffraction pattern of **1** is in good agreement with the simulated result, indicating that it is a pure phase. The ratio of Gd to Yb (1 : 9) in **1** is verified by inductively coupled plasma-mass spectrometry (Table S2) and energy-dispersive X-ray spectroscopy (Fig. S1). Further, the elemental maps of **1** (Fig. 1c) demonstrate that Gd and Yb have a homogeneous distribution. The low-temperature DC magnetic susceptibility of **1** was measured at 3–10 K under an applied field of 1000 Oe. As shown in Fig. 1d, **1** follows Curie–Weiss behavior, with a Weiss constant θ = −0.122 K for **1**, indicating weak antiferromagnetic interactions. To examine the nature of Yb–Gd interaction in **1**, low-temperature magnetic susceptibilities of $K(Gd_{0.1}Y_{0.9})_3F_{10}$ and $K(Lu_{0.1}Yb_{0.9})_3F_{10}$ (Fig. S2) are also investigated, where the $\chi_m T - T$ trends and Curie–Weiss fits demonstrate antiferromagnetic interaction in $K(Gd_{0.1}Lu_{0.9})_3F_{10}$ and $K(Y_{0.1}Yb_{0.9})_3F_{10}$. By subtracting the susceptibility data of $K(Gd_{0.1}Lu_{0.9})_3F_{10}$ and $K(Y_{0.1}Yb_{0.9})_3F_{10}$ from that of **1**, the contribution of the effect of the Gd–Gd and Yb–Yb interactions was removed. The resulting subtracted curve shows an upturn with a positive Weiss constant of θ = +0.776 K, clearly indicating a ferromagnetic nature of Yb–Gd interaction in **1**. The coexistence of competing ferromagnetic and antiferromagnetic interactions, combined with substitutional disorder, likely suppresses long-range magnetic ordering down to very low temperatures.[25]

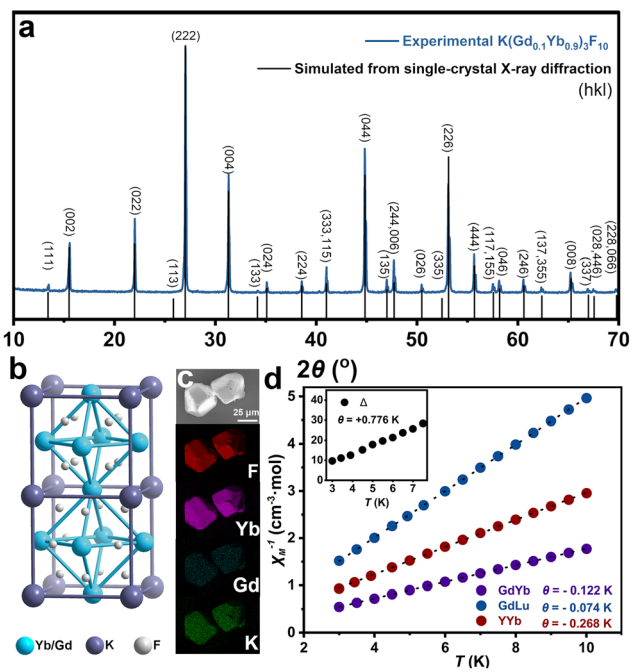

Fig. 1 (a) PXRD of **1**; (b) the crystal structure of **1**; (c) elemental mapping of **1**; (d) magnetic susceptibility and Curie–Weiss fit at 3–10 K for **1** and its analogs.

2.2 Magnetocaloric effect of $K(Gd_{0.1}Yb_{0.9})_3F_{10}$

Low-temperature heat capacity (C_p) measurements of **1** were performed to ascertain its T_0 and $-\Delta S_m$. As shown in Fig. 2a, an applied magnetic field splits the Kramers doublet of Yb^{3+} into the j_z = +1/2 and j_z = −1/2 levels, which gives rise to a

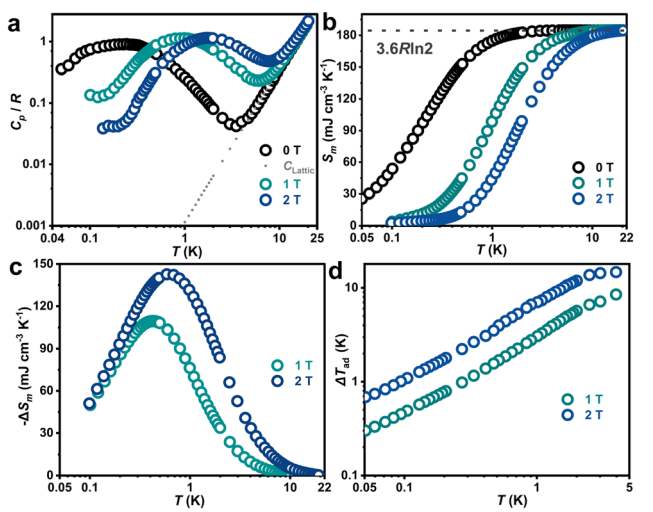

Fig. 2 (a) Experimental heat capacity (C_p) normalized to the gas constant (R) of **1**; (b) the experimental magnetic entropy S_m in **1** under various applied fields; (c) the calculated $-\Delta S_m$ values of **1** from heat capacity; (d) ΔT_{ad} values of **1** from heat capacity.

Schottky anomaly that shifts to higher temperatures with increasing field.[22] C_p values in higher temperatures (5–20 K) are dominated by lattice contributions, yielding the lattice heat capacity obeying Debye's model and a Debye temperature of 133 K. Meanwhile magnetic contributions play a crucial role in lower temperatures and magnetic heat capacity (C_m) was calculated by subtracting the lattice component from the total heat capacity, where no long-range ordering can be observed down to 0.05 K (*i.e.* $T_0 < 0.05$ K). The apparent deviation between T_0 and the Curie–Weiss constant implies the presence of competing magnetic interaction and/or disorder. As shown in Fig. 2b, the magnetic entropy (S_m) can be obtained using the relation $S_m = \int C_m/T dT$, yielding S_m that saturates at 185 mJ cm^{-3} K^{-1} at higher temperatures, consistent with the expected value of $3.6R\ln 2$ (2.7 Yb^{3+} and 0.3 Gd^{3+}). Subsequently, $-\Delta S_m$ values of **1** can be calculated by subtracting S_m (0 T) from different S_m (1 T and 2 T), resulting in the maximum $-\Delta S_m$ values of 110 mJ cm^{-3} K^{-1} at 1 T and 143 mJ cm^{-3} K^{-1} at 2 T (Fig. 2c). Notably, as evidenced by its adiabatic temperature change (ΔT_{ad}) data, ultralow temperatures down to 50 mK can be achieved through adiabatic demagnetization (Fig. 2d), starting from initial temperatures of 0.3 and 0.7 K under applied magnetic fields of 1 and 2 T, respectively.

In mapping the polarization of the cosmic microwave background missions, such as LiteBIRD, TES detectors must operate below 300 mK to maintain the required high sensitivity.[6,29,30] Table 1 summarizes several potential magnetic refrigerants capable of working below 1 K and presents their T_0, magnetic ion density (N), and $-\Delta S_m$ values in the 0.3–1.0 K range. Among these materials, **1** stands out by exhibiting large $-\Delta S_m$ values in this temperature window, only falling behind those in $Gd_{0.1}Yb_{0.9}F_3$. Particularly, its $-\Delta S_m$ is more than three times greater than that of the commercial CPA, confirming that **1** can deliver sufficient cooling capacity below 1 K. High magnetic ion density and large spin values generally enhance exchange and dipolar interactions, resulting in elevated T_0, as seen in $YbPt_2Sn$, $YbNi_{1.6}Sn$, $Gd_{0.1}Yb_{0.9}F_3$, and $KBaGd(BO_3)_2$. To suppress T_0, the magnetic lattice is often diluted with non-magnetic components; however, this strategy typically leads to a pronounced reduction in $-\Delta S_m$, as exemplified by $(NH_4)Fe(SO_4)_2{\cdot}12H_2O$ (FAA), CPA and $Gd_2(SO_4)_3{\cdot}8H_2O$ (Fig. S3). In contrast, partial Gd^{3+} substitution in KYb_3F_{10} allows **1** to preserve a high magnetic ion density while maintaining a low T_0 through competing magnetic interactions, thereby delivering substantial $-\Delta S_m$ values at ultralow temperatures.

2.3 Quasi-adiabatic demagnetization cooling in a two-stage refrigerator

Encouraged by these results, we constructed a two-stage adiabatic demagnetization refrigerator (Fig. 3a) to further evaluate the cooling performance of **1** and assess its feasibility for practical applications, with particular focus on the minimum achievable temperature and cooling capacity.[37] In ADR integration, **1** was mixed with high-purity Ag powder and pressed into dense buttons. The incorporation of Ag is a standard practice, as most inorganic magnetic refrigerants exhibit limited intrinsic thermal conductivity at low temperatures. The metallic network formed by Ag significantly enhances the effective thermal transport within the refrigerant pill, ensuring rapid internal thermal equilibration and efficient heat exchange during demagnetization cycles. For sufficient cooling output, a salt pill containing 143.8 g of **1** (contained in pressed salt and silver buttons) was prepared by loading the buttons into a copper cylinder and housing the assembly within an aluminum alloy sleeve (Fig. S4). The salt pill has a diameter of 36 mm and a height of 81 mm (the portion containing **1**), and is housed within a magnet bore with an inner diameter of 50 mm and a height of 136 mm. A copper finger extending below the magnet serves as the cold head and can be extended both horizontally and vertically as required (capable of reaching a diameter exceeding 200 mm). The two-stage ADR: in this configuration, adiabatic demagnetization of GGG in the first stage precools the second stage below 1 K.[38] The first-stage heat switch is a commercial active gas-gap

Table 1 T_0, N and $-\Delta S_m$ values of selected refrigerants in 0.3–1 K at 2 T

Refrigerants	T_0 (K)	N (10^{21} cm^{-3})	$-\Delta S_m$ (mJ cm^{-3} K^{-1})			
			0.3 K	0.5 K	0.7 K	1.0 K
$Gd_{0.1}Yb_{0.9}F_3$ [26]	0.18	21.2	164	193	197	183
$K(Gd_{0.1}Yb_{0.9})_3F_{10}$	**<0.05**	**16.1**	**122**	**140**	**142**	**132**
KYb_3F_{10} [28]	<0.05	16.1	127	133	128	115
$LiYb_{0.9}Gd_{0.1}F_4$ [25]	0.085	14.2	111	132	136	128
$Yb_3Ga_5O_{12}$ [24]	0.054, 0.18	13.2	95	113	116	112
$KBaYb(BO_3)_2$ [22,31]	0.009	6.72	60	61	58	51
$NaYbP_2O_7$ [21]	—	6.6	—	57	54	48
$Na_2BaCo(PO_4)_2$(4 T) [23]	0.15	5.8	25	32	37	42
$KBaGd(BO_3)_2$ [32,33]	0.263	6.53	116	144	145	134
$YbPt_2Sn$ [34]	0.25	12.6	50	80	86	93
$YbNi_4Mg$ [35]	0.3	11.5	29	53	67	71
$Gd_2(SO_4)_3{\cdot}8H_2O$	0.18	4.88	78	105	112	108
$(NH_4)Fe(SO_4)_2{\cdot}12H_2O$ [36]	0.026	2.14	51	52	50	45
$CrK(SO_4)_2{\cdot}12H_2O$ [36]	0.009	2.20	40	40	39	34

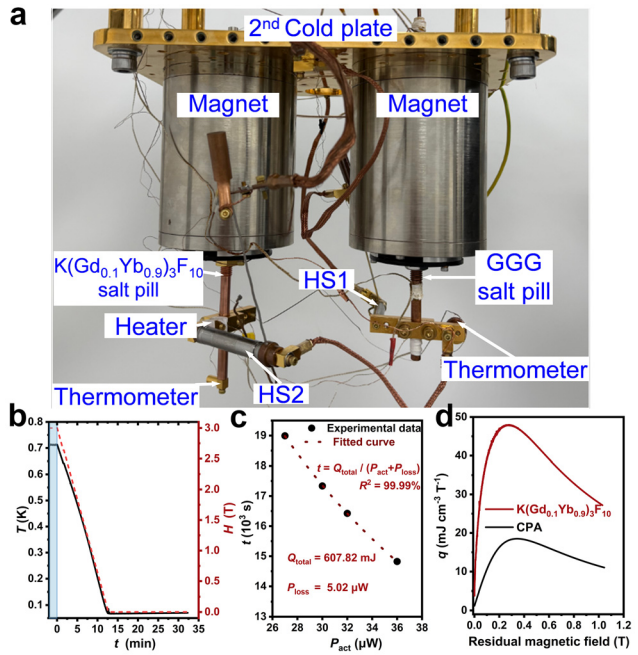

Fig. 3 (a) The two-stage adiabatic demagnetization refrigerator; (b) the adiabatic demagnetization cooling of **1**; (c) time-load data of isothermal demagnetization; (d) specific cooling capacity q of **1** compared with commercial CPA at 300 mK.

switch (Chase), while the second stage employs a home-made active gas-gap switch (Fig. S5). Both superconducting magnets can generate fields up to 4 T. As shown in Fig. 3b, a minimum temperature of 67 mK was achieved from an initial temperature of 0.712 K at a field of 3 T, and this value remained nearly unchanged under slight variations of the starting temperature. The stable attainment of 67 mK also reflects the low heat leakage in the system, including contributions from eddy-current heating, heat switch leakage, suspension conduction, and lead conduction. The cooling capacity at 300 mK was further quantified by applying controlled heating powers (P_{act}) to the copper rod. Accounting for unknown heat loss (P_{loss}), the total cooling capacity (Q_{total}) was calculated using $Q_{total} = (P_{act} + P_{loss}) \times t$. From the holding times corresponding to heating powers of 27, 30, 32, and 36 μW during isothermal demagnetization, Q_{total} was fitted to be 607.82 mJ with P_{loss} = 5.02 μW (Fig. 3c). The above results also imply that the two-stage ADR system can sustain an ultralow temperature of 300 mK for over 30 h under free-load conditions (P_{act} = 0). Since the cooling capacity of most reported magnetic refrigerants has not been investigated under practical refrigeration conditions, comparisons are therefore mainly made with the commercial CPA. For a fair comparison of the cooling performance between **1** and CPA, we introduce the specific cooling capacity (the definition is described in the SI). The maximum specific cooling capacity of **1** during the 300 mK isothermal magnetization process is 47.99 mJ cm^{-3} T^{-1}, far exceeding that of the commercial refrigerant CPA (Fig. 3d). It is worth noting that although the specific cooling capacity of **1** is comparable to that of $LiGd_{0.1}Yb_{0.9}F_4$ we reported previously,[25] the observed minimum temperature of 67 mK for **1** is markedly lower than the 160 mK achieved with $LiGd_{0.1}Yb_{0.9}F_4$, demonstrating that **1** is a promising sub-kelvin refrigerant. We noted that although the ADR performance of $Yb_3Ga_5O_{12}$ has been investigated under load conditions, the available data do not allow a quantitative assessment of its specific cooling capacity.[39] In contrast, **1** satisfies application scenarios demonstrated by $Yb_3Ga_5O_{12}$; for example, a cooling power of 50 μW at 300 mK is provided for 1 h,[24] whereas **1** can remain stable for 3 hours at 300 mK under the same load, further underscoring its efficiency and feasibility in practical ADR operations. In addition, classical hydrated paramagnetic salts typically require growth on Cu or Au wires and careful encapsulation to prevent dehydration and degradation, imposing stringent requirements on packaging procedures and long-term stability.[9] By contrast, the present material can be directly mixed with silver powder and pressed into pellets, providing mechanical robustness, enhanced thermal contact, and good stability (Fig. S6 and S7) without special encapsulation protocols. This simplified processing not only facilitates practical implementation but also reduces overall fabrication cost.

Significantly, the combination of the giant $-\Delta S_m$ values in **1** and the high efficiency of its salt pill (reaching ~90% of the theoretical value) enables the system employing **1** together with GGG to achieve an extended zero-load hold time of over 30 h and a large cooling capacity of 607.82 mJ at 300 mK, thereby meeting diverse practical cooling power requirements. Most notably, if the loading of **1** was increased to 358.4 g, the refrigerator can achieve a cooling capacity at 300 mK comparable to that of the GL7 sorption cooler containing 2 L of ^{3}He,[40] thereby demonstrating the potential of ADR with large-capacity refrigerants as a practical alternative to ^{3}He-based sorption refrigeration.

3 Conclusions

In summary, we have prepared a magnetic refrigerant of $K(Gd_{0.1}Yb_{0.9})_3F_{10}$ (**1**) *via* partial substitution of Gd^{3+} into KYb_3F_{10}. Heat-capacity measurements indicate the absence of long-range magnetic ordering down to 50 mK and reveal substantial $-\Delta S_m$ across the 0.3–1.0 K range. When integrated into a two-stage ADR system, **1** reached a minimum temperature of 67 mK and delivered a high specific cooling capacity of 47.99 mJ cm^{-3} T^{-1} under 0.27 T, establishing it as a promising sub-kelvin refrigerant that rivals ^{3}He-based systems. Beyond demonstrating a cooling method comparable to ^{3}He sorption refrigeration near 300 mK, this work provides a robust foundation for advancing magnetic refrigeration as a practical helium-free alternative to support the development of quantum technologies.

4 Experimental

4.1 Synthesis of $K(Yb_{0.9}Gd_{0.1})_3F_{10}$ (1)

$YbCl_3{\cdot}6H_2O$ (0.349 g, 0.9 mmol), $GdCl_3{\cdot}6H_2O$ (0.037 g, 0.1 mmol) and KCl (0.596 g, 8 mmol) were added to 15 mL of

distilled water and stirred to thoroughly dissolve before the dropwise addition of hydrofluoric acid (0.16 mL, ~4 mmol). Subsequently, the mixture was sealed in a 25 mL Teflon-lined stainless steel container and heated at 180 °C for 3 days. The pure crystalline $K(Yb_{0.9}Gd_{0.1})_3F_{10}$ (**1**) was obtained after washing with distilled water three times and drying at 80 °C overnight. Yield: 161.3 mg, 65.09% based on Yb.

4.2 Synthesis of $K(Yb_{0.9}Y_{0.1})_3F_{10}$

The preparation of $K(Yb_{0.9}Y_{0.1})_3F_{10}$ is quite similar to **1** except that the dosage of $GdCl_3{\cdot}6H_2O$ (0.037 g, 0.1 mmol) was changed as $YCl_3{\cdot}6H_2O$ (0.030 g, 0.1 mmol).

4.3 Synthesis of $K(Lu_{0.9}Gd_{0.1})_3F_{10}$

The preparation of $K(Lu_{0.9}Gd_{0.1})_3F_{10}$ is quite similar to **1** except that the dosage of $YbCl_3{\cdot}6H_2O$ (0.349 g, 0.9 mmol) was adjusted as $LuCl_3{\cdot}6H_2O$ (0.350 g, 0.9 mmol).

4.4 Scale-up synthesis of $K(Yb_{0.9}Gd_{0.1})_3F_{10}$ (1)

$YbCl_3{\cdot}6H_2O$ (69.75 g, 0.18 mol) and $GdCl_3{\cdot}6H_2O$ (7.434 g, 0.02 mol) were added to 600 mL of distilled water and stirred to thoroughly dissolve before dropwise addition of KF (41.832 g, 0.72 mol). Subsequently, the mixture was sealed in a 1000 mL Teflon-lined stainless steel container and heated at 180 °C for 3 days. The crystalline **1** (Fig. S6–S9) was obtained after washing with distilled water five times and drying at 80 °C overnight. Yield: 41.366 g, 83.46% based on Yb.

4.5 Salt pill fabrication

The salt pill consists of a copper heat-transfer rod, **1** buttons (prepared by pressing a mixture of **1** and silver powder in equal mass), and an aluminum-alloy sleeve. Prior to installation, a thin layer of Apiezon N grease was applied to the surface of **1** button to ensure good thermal contact with the cavity of the copper rod. The cavity was machined with axial slots, both to facilitate easier loading of the refrigerant and to suppress eddy current heating in the copper. Finally, the aluminum-alloy sleeve was fitted over the copper cavity to complete the assembly.

During assembly at room temperature, the salt buttons were mounted using an interference fit. Upon cooling, the contraction of the metal generates sufficient pressure to ensure effective thermal contact between **1** button and the copper heat-transfer rod in the cryogenic environment. A total of 143.8 g of **1** was loaded into the salt pill. To simulate operation under thermal load, a resistive heater was affixed to the copper rod.

4.6 Specific cooling capacity

The cooling performance of magnetocaloric materials is related to the operating temperature, material volume, and applied magnetic field. To ensure a fair comparison between the cooling performance of **1** and CPA, the specific cooling capacity of **1** (q_1) during isothermal demagnetization from magnetic field x to zero field is defined by the following equation:

$$q_1 = \frac{(P_{act} + P_{loss})\cdot t_x}{x\cdot V}$$

where x denotes the magnetic field at the start of isothermal demagnetization, t_x represents the corresponding refrigeration duration, and V is the volume of the pure material **1** used. As shown in Fig. 3c, the fitted heat leak is determined as P_{loss} = 5.02 μW. The specific cooling capacity P_1 is calculated by substituting test data obtained at P_{act} = 30 μW into the above equation.

The specific cooling capacity of CPA (q_{CPA}) is obtained by the following formula:

$$q_{CPA} = \frac{T\cdot(S_{0T} - S_x)}{x}$$

where T is the isothermal demagnetization temperature (300 mK in this study); S_{0T} is the theoretical entropy per unit volume of CPA at zero magnetic field, and S_x is the theoretical entropy per unit volume of CPA at the same magnetic field x.

Author contributions

Q.-F. Xu and P. Zhao contributed equally to this work. L.-S. Long and L.-S. Zheng conceived the work. Q.-F. Xu and R.-T. Wu prepared the samples and conducted the magnetocaloric and specific heat data analysis. M.-T. Chen performed magnetic measurements. P. Zhao and W. Dai designed the salt pill, the two-stage adiabatic demagnetization refrigerator and did related experiments. All authors participated in the discussion and the revision of the manuscript.

Conflicts of interest

There are no conflicts to declare.

Data availability

The data supporting this article have been included as part of the supplementary information (SI).

Supplementary information: measurement methods, X-ray crystallography, crystal data, powder X-ray diffraction data, energy-dispersive X-ray spectroscopy, and ICP results. See DOI: https://doi.org/10.1039/d6im00032k.

CCDC 2523489 (**1**) contains the supplementary crystallographic data for this paper.[41]

Acknowledgements

This work was supported by the National Natural Science Foundation of China (grant no. 22527801, 92161203 and 92361301), and the Postdoctoral Fellowship Program of China Postdoctoral Science Foundation (grant no. GZC20240894 and 2024M761764). The authors thank Dr. Chao Zhang from the Instrumentation and Service Center for Physical Sciences at Westlake University for measurements of heat capacity and magnetism.

References

1 Y. Z. Zheng, G. J. Zhou, Z. Zheng and R. E. P. Winpenny, Molecule-based magnetic coolers, *Chem. Soc. Rev.*, 2014, **43**, 1462–1475.
2 S. J. Liu, S. D. Han, J. P. Zhao, J. Xu and X. H. Bu, In-situ synthesis of molecular magnetorefrigerant materials, *Coord. Chem. Rev.*, 2019, **394**, 39–52.
3 G. Lorusso, J. W. Sharples, E. Palacios, O. Roubeau, E. K. Brechin, R. Sessoli, A. Rossin, F. Tuna, E. J. L. McInnes, D. Collison and M. Evangelisti, A dense metal-organic framework for enhanced magnetic refrigeration, *Adv. Mater.*, 2013, **25**, 4653–4656.
4 X. Y. Zheng, X. J. Kong, Z. Zheng, L. S. Long and L. S. Zheng, High-nuclearity lanthanide-containing clusters as potential molecular magnetic coolers, *Acc. Chem. Res.*, 2018, **51**, 517–525.
5 J. M. Duval, T. Prouvé, P. Shirron, K. Shinozaki, Y. Sekimoto, T. Hasebe, G. Vermeulen, J. André, M. Hasumi, L. Montier and B. Mot, LiteBIRD cryogenic chain: 100 mK cooling with mechanical coolers and ADRs, *J. Low Temp. Phys.*, 2020, **199**, 730–736.
6 C. Jiang, C. Li, H. Jin and W. Cui, Development of adiabatic demagnetization refrigerator for the HUBS mission, *Sci. Bull.*, 2023, **68**, 2709–2711.
7 W. P. Halperin, The impact of helium shortages on basic research, *Nat. Phys.*, 2014, **10**, 467–470.
8 Q. F. Xu, R. T. Wu, L. S. Long and L. S. Zheng, Ultralow-temperature magnetic refrigeration inorganic materials: From designed synthesis to adiabatic demagnetization refrigeration, *Acc. Chem. Res.*, 2025, **58**, 2898–2909.
9 P. J. Shirron and D. McCammon, Salt pill design and fabrication for adiabatic demagnetization refrigerators, *Cryogenics*, 2014, **62**, 163–171.
10 P. J. Shirron, Applications of the magnetocaloric effect in single-stage, multi-stage and continuous adiabatic demagnetization refrigerators, *Cryogenics*, 2014, **62**, 130–139.
11 T. Esat, P. Borgens, X. Yang, P. Coenen, V. Cherepanov, A. Raccanelli, F. S. Tautz and R. Temirov, A millikelvin scanning tunneling microscope in ultra-high vacuum with adiabatic demagnetization refrigeration, *Rev. Sci. Instrum.*, 2021, **92**, 063701.
12 W. P. Chen, J. Singleton, L. Qin, A. Camón, L. Engelhardt, F. Luis, R. E. P. Winpenny and Y.-Z. Zheng, Quantum Monte Carlo simulations of a giant $\{Ni_{21}Gd_{20}\}$ cage with a S = 91 spin ground state, *Nat. Commun.*, 2018, **9**, 2107.
13 Q. Guo, W. Ren, P. Liu, J. Yao, J. Xiang, K. Zhang, Y. Wang, L. S. R. Kumara, X. Wang, W. Li and B. Li, Giant low-field magnetocaloric effect at sub-Kelvin temperatures in ferromagnetic NH_4GdF_4, *J. Am. Chem. Soc.*, 2025, **147**, 34862–34868.
14 E. C. Koskelo, C. Liu, P. Mukherjee, N. D. Kelly and S. E. Dutton, Free-spin dominated magnetocaloric effect in dense Gd^{3+} double perovskites, *Chem. Mater.*, 2022, **34**, 3440–3450.
15 I. Tejedor, D. E. Kravchenko, J. Gandara-Loe, R. Ameloot, I. Gascón and O. Roubeau, Gd metal–organic framework thin film for on-chip local magnetic refrigeration, *Chem. Mater.*, 2024, **36**, 8239–8246.
16 B. Wang, X. Liu, F. Hu, J. Wang, J. Xiang, P. Sun, J. Wang, J. Sun, T. Zhao, Z. Mo, J. Shen, Y. Chen, Q. Huang and B. Shen, A record-high cryogenic magnetocaloric effect discovered in $EuCl_2$ compound, *J. Am. Chem. Soc.*, 2024, **146**, 35016–35022.
17 Y. Wang, J. Xiang, L. Zhang, J. Gong, W. Li, Z. Mo and J. Shen, Giant low-field cryogenic magnetocaloric effect in a polycrystalline EuB_4O_7 compound, *J. Am. Chem. Soc.*, 2024, **146**, 3315–3322.
18 T. Numazawa, K. Kamiya, P. Shirron, M. DiPirro and K. Matsumoto, Magnetocaloric effect of polycrystal $GdLiF_4$ for adiabatic magnetic refrigeration, *AIP Conf. Proc.*, 2006, 1579–1580.
19 P. J. Shirron, M. O. Kimball, B. L. James, D. C. Wegel, R. M. Martinez, R. L. Faulkner, L. Neubauer and M. Sansebastian, Design and predicted performance of the 3-stage ADR for the Soft-X-ray Spectrometer instrument on Astro-H, *Cryogenics*, 2012, **52**, 165–171.
20 J. Peter, Shirron, Applications of the magnetocaloric effect in single-stage, multi-stage and continuous adiabatic demagnetization refrigerators, *Cryogenics*, 2014, **62**, 130–139.
21 U. Arjun, K. M. Ranjith, A. Jesche, F. Hirschberger, D. D. Sarma and P. Gegenwart, Efficient adiabatic demagnetization refrigeration to below 50 mK with ultrahigh-vacuum-compatible ytterbium diphosphates $AYbP_2O_7$ (A=Na, K), *Phys. Rev. Appl.*, 2023, **20**, 014013.
22 Y. Tokiwa, S. Bachus, K. Kavita, A. Jesche, A. A. Tsirlin and P. Gegenwart, Frustrated magnet for adiabatic demagnetization cooling to milli-Kelvin temperatures, *Commun. Mater.*, 2021, **2**, 42.
23 J. Xiang, C. Zhang, Y. Gao, W. Schmidt, K. Schmalzl, C.-W. Wang, B. Li, N. Xi, X.-Y. Liu, H. Jin, G. Li, J. Shen, Z. Chen, Y. Qi, Y. Wan, W. Jin, W. Li, P. Sun and G. Su, Giant magnetocaloric effect in spin supersolid candidate $Na_2BaCo(PO_4)_2$, *Nature*, 2024, **625**, 270–275.
24 D. A. Paixao Brasiliano, J.-M. Duval, C. Marin, E. Bichaud, J.-P. Brison, M. Zhitomirsky and N. Luchier, YbGG material for Adiabatic Demagnetization in the 100mK–3K range, *Cryogenics*, 2020, **105**, 103002.
25 Q. Xu, P. Zhao, M. Chen, R. Wu, W. Dai, L. Long and L. Zheng, Exceptional cooling capacity of $LiGd_{0.1}Yb_{0.9}F_4$ at sub-Kelvin temperatures, *Adv. Mater.*, 2025, **37**, 2414226.
26 Q. F. Xu, M. T. Chen, R. T. Wu, L. S. Long and L. S. Zheng, Achieving magnetic refrigerants with large magnetic entropy changes and low magnetic ordering temperatures, *J. Am. Chem. Soc.*, 2024, **146**, 20116–20121.
27 J. W. Pierce and Y. P. Hong, Proceedings of the tenth rare earth research conference, Carefree, Arizona; U.S. Atomic energy commission, technical information center: Oak Ridge, TN, 1973, p. 529.
28 Q. F. Xu, X. Y. Liu, R. T. Wu, M. Y. Fu, M. T. Chen, J. S. Xiang, Y. S. Meng, T. Liu, P. J. Sun, L. S. Long and L. S. Zheng, Temperature below 30 mK achieved by adiabatic demagnetization refrigeration, *J. Am. Chem. Soc.*, 2025, **147**, 27089–27094.

29 A. Coppolecchia, L. Lamagna, S. Masi, P. A. R. Ade, G. Amico, E. S. Battistelli, P. De Bernardis, F. Columbro, L. Conversi, G. D'Alessandro, M. De Petris, M. Gervasi, F. Nati, L. Nati, A. Paiella, F. Piacentini, G. Pisano, G. Presta, A. Schillaci, C. Tucker and M. Zannoni, The long duration cryogenic system of the OLIMPO balloon–borne experiment: Design and in–flight performance, *Cryogenics*, 2020, **110**, 103129.

30 L. Duband, T. Prouve, J. Bock, L. Moncelsi and A. Schillaci, Sub-Kelvin cooling for the BICEP array project, *arXiv*, 2020, preprint, arXiv:2009.09997, DOI: 10.48550/ARXIV.2009.09997.

31 T. Treu, M. Klinger, N. Oefele, P. Telang, A. Jesche and P. Gegenwart, Utilizing frustration in Gd- and Yb-based oxides for milli-kelvin adiabatic demagnetization refrigeration, *J. Phys.: Condens. Matter*, 2025, **37**, 013001.

32 Z. M. Song, N. Zhao, H. Ge, T. T. Li, J. Yang, L. Wang, Y. Fu, Y. Z. Zhang, S. M. Wang, J. W. Mei, H. He, S. Guo, L. S. Wu and J. M. Sheng, Magnetic phase diagrams and large magnetocaloric effects of the two-dimensional antiferromagnetic triangular lattice of Gd^{3+} ions in $KBaGd(BO_3)_2$, *Phys. Rev. B*, 2023, **107**, 125126.

33 A. Jesche, N. Winterhalter-Stocker, F. Hirschberger, A. Bellon, S. Bachus, Y. Tokiwa, A. A. Tsirlin and P. Gegenwart, Adiabatic demagnetization cooling well below the magnetic ordering temperature in the triangular antiferromagnet $KBaGd(BO_3)_2$, *Phys. Rev. B*, 2023, **107**, 104402.

34 D. Jang, T. Gruner, A. Steppke, K. Mitsumoto, C. Geibel and M. Brando, Large magnetocaloric effect and adiabatic demagnetization refrigeration with $YbPt_2Sn$, *Nat. Commun.*, 2015, **6**, 8680.

35 X. Zhang, T. Zhang, Z. Zhuang, Z. Leng, Z. Wei, X. Liu, J. Xiang, S. Zhang and P. Sun, $YbNi_4Mg$: Superheavy fermion with enhanced Wilson ratio and magnetocaloric effect, *Phys. Rev. Mater.*, 2025, **9**, 014402.

36 O. E. Vilches and J. C. Wheatley, Measurements of the specific heats of three magnetic salts at low temperatures, *Phys. Rev.*, 1966, **148**, 509–516.

37 Y. Wang, P. Zhao, Y. Li, K. Li and W. Dai, Performance characterization of a large CPA salt pill in an ADR refrigerator, *Cryogenics*, 2026, **157**, 104318.

38 P. Zhao, K. Li, Y. Li, W. Dai and J. Shen, The performance of GGG salt pill with heat transfer via ^3He, *Cryogenics*, 2025, **151**, 104182.

39 J. M. Duval, A. Attard and D. A. P. Brasiliano, Experimental results of ADR cooling tuned for operation at 50 mK or higher temperature, *IOP Conf. Ser.: Mater. Sci. Eng.*, 2020, **755**, 012122.

40 CHASE RESEARCH CRYOGENICS LIMITED. GL7-performance-notes, https://www.chasecryogenics.com/, (accessed March 24, 2026).

41 CCDC 2523489: Experimental Crystal Structure Determination, 2026, DOI: 10.25505/fiz.icsd.cc2qpww6.